Protein Science (1999), *8*:1888–1898. Cambridge University Press. Printed in the USA.

Histidine placement in de novo–designed heme proteins

BRIAN R. GIBNEY AND P. LESLIE DUTTON

The Johnson Research Foundation, Department of Biochemistry and Biophysics, School of Medicine, University of Pennsylvania, B501 Richards Building, Philadelphia, Pennsylvania 19104

(RECEIVED November 16, 1998; ACCEPTED May 26, 1999)

Abstract

The effects of histidine residue placement in a de novo-designed four-α-helix bundle are investigated by placement of histidine residues at coiled coil heptad **a** positions in two distinct heptads and at each position within a single heptad repeat of our prototype heme protein maquette, $[H10H24]_2$ [{*Ac*-CGGGELWKL·**H**EELLKK·FEELLKL·**H**EERLKK·L-$CONH_2$}$_2$]$_2$ composed of a generic (α-SS-α)$_2$ peptide architecture. The heme to peptide stoichiometry of variants of $[H10H24]_2$ with either or both histidines on each helix replaced with noncoordinating alanine residues ($[H10A24]_2$, $[A10H24]_2$, and $[A10A24]_2$) demonstrates the obligate requirement of histidine for biologically significant heme affinity. Variants of $[A10A24]_2$, [{*Ac*-CGGGELWKL·**A**EELLKK·FEELLKL·**A**EERLKK·L-$CONH_2$}$_2$]$_2$, containing a single histidine per helix in positions 9 to 15 were evaluated to verify the design based on molecular modeling. The *bis*-histidine site formed between heptad positions **a** at 10 and 10′ bound ferric hemes with the highest affinity, K_{d1} and K_{d2} values of 15 and 800 nM, respectively. Placement of histidine at position 11 (heptad position **b**) resulted in a protein that bound a single heme with moderate affinity, K_{d1} of 9.5 μM, whereas the other peptides had no measurable apparent affinity for ferric heme with K_{d1} values $>$200 μM. The *bis*-histidine ligation of heme to $[H10A24]_2$ and $[H11A24]_2$ was confirmed by electron paramagnetic resonance spectroscopy. The protein design rules derived from this study, together with the narrow tolerances revealed, are applicable for improving future heme protein designs, for analyzing the results of randomized heme protein combinatorial libraries, as well as for implementation in automated protein design.

Keywords: de novo design; electrochemistry; heme protein; maquette; metalloprotein

Metalloproteins compose >30% of the named proteins (IUBAB, 1992) and, consistent with their ubiquitous nature, serve numerous and diverse chemical functions in biological systems. Recently, rational (Bryson et al., 1995) and combinatorial (Kamtekar et al., 1993) protein design strategies have recognized the importance of metals in proteins and have evolved to include the incorporation of transition metals in an effort to access their structural (Ghadiri & Choi, 1990; Regan & Clarke, 1990), regulatory (Dieckmann et al., 1997, 1998), catalytic (Pinto et al., 1997), and electron transfer (Choma et al., 1994; Mutz et al., 1996; Kozlov & Ogawa, 1997; Rau et al., 1998; Sharp et al., 1998) properties (Gibney et al., 1997b; Lu & Valentine, 1997; Hellinga, 1998b). These studies promise future metal ion chemical reactivity of the types observed by natural metalloproteins, for example, Lewis acid hydrolysis (Lipscomb & Sträter, 1996) and organic substrate oxidation (Hayashi, 1962). Research in the de novo design of proteins has provided preliminary engineering specifications for the assembly of stable and conformationally specific proteins (Munson et al., 1994, 1996; Dolphin et al., 1996; Gibney et al., 1997c; Jiang et al., 1997; Roy et al., 1997; Schafmeister et al., 1997; Bryson et al., 1998; Hill & DeGrado, 1998; Johansson et al., 1998; Skalicky et al., 1999) based on coiled coil (Crick, 1953) and four-α-helical bundle frameworks that are common architectural motifs of metalloproteins being found as independent units (Ward et al., 1975; Finzel et al., 1985; deMaré et al., 1996) or as components of larger proteins (Nordlund et al., 1990; Rosenzweig et al., 1993). These designs are typically based on the periodic seven amino acid or heptad repeat of polar and apolar residues, ($\mathbf{a}_{apolar}$-$\mathbf{b}_{polar}$-$\mathbf{c}_{polar}$-$\mathbf{d}_{apolar}$-$\mathbf{e}_{either}$-$\mathbf{f}_{polar}$-$\mathbf{g}_{polar}$)$_n$, which fold into an aggregate of amphiphilic helices (Fig. 1). The incorporation of redox metals and biological cofactors into these scaffolds yields *maquettes* (Robertson et al., 1994), simplified protein structures reminiscent of their much more elaborate natural counterparts.

Maquettes have been shown to offer a constructive approach to metalloprotein structure–function relationships, providing insight into the protein–protein assembly (Gibney et al., 1997a, 1997c, 1999), protein-cofactor incorporation (Rabanal et al., 1996; Mulholland et al., 1998; Sharp et al., 1998), modulation of bound cofactors by protein and adjacent cofactors (Gibney et al., 1998; Shifman et al., 1998), and modular protein design via multicofactor assembly (Gibney et al., 1996; Sharp et al., 1998). The increasing frequency of successful de novo metalloprotein designs

Reprint requests to: P. Leslie Dutton, Department of Biochemistry and Biophysiology, University of Pennsylvania, B501 Richards Building, Philadelphia, Pennsylvania 19104; e-mail: dutton@mail.med.upenn.edu.

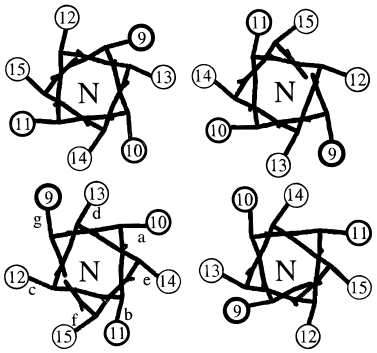

```
                cdefg•abcdefg•abcdefg•abcdegf•a
H10H24      CGGGELWKL•HEELLKK•FEELLKL•HEERLKK•L
H10A24      CGGGELWKL•HEELLKK•FEELLKL•AEERLKK•L
A10H24      CGGGELWKL•AEELLKK•FEELLKL•HEERLKK•L
A10A24      CGGGELWKL•AEELLKK•FEELLKL•AEERLKK•L

H9A24       CGGGELWKH•AEELLKK•FEELLKL•AEERLKK•L
H10A24      CGGGELWKL•HEELLKK•FEELLKL•AEERLKK•L
H11A24      CGGGELWKL•AHELLKK•FEELLKL•AEERLKK•L
H12A24      CGGGELWKL•AEHLLKK•FEELLKL•AEERLKK•L
H13A24      CGGGELWKL•AEEHLKK•FEELLKL•AEERLKK•L
H14A24      CGGGELWKL•AEELHKK•FEELLKL•AEERLKK•L
H15A24      CGGGELWKL•AEELLHK•FEELLKL•AEERLKK•L
```

Fig. 1. Helical wheel diagram of a single heptad (positions 9–15) of $[H10A24]_2$, shown as a generic all-parallel four-helix bundle, together with a sequence alignment of the peptides studied. The heptads are indicated in the primary sequences by bullets.

(Benson et al., 1998; Farinas & Regan, 1998) including the assembly of different redox cofactors into the same peptide represents a growing understanding of the protein ligand requirements for metal ion incorporation. Although the proper placement of suitable amino acid ligands within a stable protein scaffold is inherent to these successful metalloprotein designs, systematic studies of the optimal ligand placement (design specifications) and the limits of error (design tolerances) in designed proteins are limited (Klemba & Regan, 1995; Hellinga, 1998a). Such studies are critical to evaluating metalloprotein designs because the requisite potentials and force fields for molecular modeling of metals are not as well developed as those for organic systems. Maquettes offer a framework in which to study the fundamental relationship between the prosthetic group and the surrounding protein ligands forming a foundation toward the greater challenge of manipulating the chemistry at these internal metal sites.

Herein, we have utilized $[H10A24]_2$ (Fig. 1) to explore the placement of histidine residues to provide a more complete understanding of the ligand engineering specifications for optimal heme affinity in designed proteins. Within a homotetrameric four-α-helix bundle assembly, a single histidine residue was placed at each position of a continuous heptad from H9 to H15 (heptad **g** to **e** positions, see Fig. 1). The resulting seven homotetrameric four-α-helix bundles, $[HxA24]_2$ (x = 9–15), each contain four histidines as potential heme ligands. Direct evidence for assembly of the peptide ligands into four-α-helix bundles is presented along with their global thermodynamic stability (measured by chemical denaturation). Each peptide is quantitatively evaluated for oxidized heme binding and the properties of the heme peptides delineated. These data indicate that the placement of the histidine ligands at heptad **a** positions is far superior to their placement elsewhere in the selected heptad.

Results

Survey of heme protein maquettes

The optimal scaffold for evaluation of heme binding competency was determined by evaluation of a series of maquettes derived from the prototype heme maquette, $[H10H24]_2$. By analogy to ubiquinol–cytochrome *c* oxidoreductase (cytochrome bc_1 complex, complex III) (Trumpower, 1990; Ding et al., 1995; Xia et al., 1997; Zhang et al., 1998) on which the design of $[H10H24]_2$ is based, the sequence has two histidine residues in interior facing heptad **a** positions (10 and 24) displaced by 14 amino acids (two heptads) as shown in Figure 1. Additionally, the phenylalanine residue at position 17 and the arginine residue at position 27 were incorporated based on sequence homologies of cytochrome bc_1 complexes. The chemically synthesized 31 amino acid peptide (α-SH) is covalently dimerized by oxidation of its N-terminal cysteine residues (α-SS-α) or [H10H24], affording a pair of *bis*-histidine heme binding sites at position 10,10′ and 24,24′. Spontaneous self-assembly of these disulfide linked di-α-helical peptides in solution as a dimer, $(\alpha\text{-SS-}\alpha)_2$ or $[H10H24]_2$, provides four *bis*-histidine heme binding sites with ferric heme K_d values measured between 50 nM and 25 μM. The global architecture of $[H10H24]_2$ is sufficient stable to permit site selected manipulation of its amino acid sequence without drastic changes in aggregation state or helical content complicating the analysis (Gibney et al., 1999). In addition, the global protein fold orients the chiral ligands, distant in primary sequence, to assume a close proximity without the necessity for an organic cosolvent as is used in some smaller heme–peptide systems (Benson et al., 1995; Arnold et al., 1997a, 1997b; D'Auria et al., 1997; Nastri et al., 1997).

Two peptides derived from replacement of the histidines with nonligating alanines, $[H10A24]_2$ and $[A10H24]_2$, were designed to test the placement of the heptad **a**–heptad **a** *bis*-histidine heme binding site within two different heptads of this peptide architecture (Fig. 1). Heme stoichiometry studies on $[H10A24]_2$ and $[A10H24]_2$ indicated that the heme:four-α-helix bundle ratio was 2:1. This is reduced from 4:1 in $[H10H24]_2$ and fully consistent with the necessity for the designed histidine ligands (Robertson et al., 1994). Evaluation of the ferric heme K_d values of the $[H10A24]_2$ and $[A10H24]_2$ peptides demonstrated substantially higher heme affinity in $[H10A24]_2$. Additionally, a peptide with both histidine residues replaced with noncoordinating alanines, $[A10A24]_2$, failed to bind oxidized heme with a K_{d1} tighter than 200 μM, the limit of the measurement, further confirming the necessity of the histidine residues for heme ligation, as designed.

$[H10A24]_2$ ligand replacements

$[H10A24]_2$ was selected over $[A10H24]_2$ as the template to study the effect of placing histidine at each position in a continuous heptad because of its 50-fold lower K_{d1} for heme. As with $[H10A24]_2$, each member of the resulting $[HxA24]_2$ (x = 9–15) peptide series contains a single histidine per helix as a potential heme ligand and, hence, four histidine residues per four-α-helix bundle. Figure 1 shows their primary sequences and demonstrates the wide range of relative histidine orientations in the series.

Table 1. *Peptide characterization*

Peptide	Molecular weight		Molar ellipticity			
	Monomer mass	Gel permeation chromatography	Θ_{222}	Θ_{208}	Ratio	% α-Helix
$[H10H24]_2$	7,575	18,600	25,600	27,000	0.95	80.1
$[H10A24]_2$	7,444	17,300	26,100	23,500	0.90	81.5
$[A10H24]_2$	7,444	17,300	26,000	29,200	0.89	83.2
$[A10A24]_2$	7,313	17,800	27,600	29,700	0.93	86.2
$[H9A24]_2$	7,444	18,200	27,500	23,400	0.85	85.9
$[H10A24]_2$	7,444	17,300	26,100	23,500	0.90	81.5
$[H11A24]_2$	7,412	17,200	28,000	23,500	0.84	87.5
$[H12A24]_2$	7,412	18,600	26,000	22,600	0.87	81.2
$[H13A24]_2$	7,444	18,400	25,000	22,700	0.91	78.1
$[H14A24]_2$	7,444	17,600	25,200	22,900	0.91	79.6
$[H15A24]_2$	7,414	18,100	26,400	23,200	0.88	82.5

Secondary structure

Figure 2 shows that the far-ultraviolet (UV) circular dichroism (CD) spectra of each of the peptides in aqueous buffer is typical of a highly α-helical peptide (78–86% helical content) with minima at 208 and 222 nm ($\pi \rightarrow \pi^*$ and $n \rightarrow \pi^*$ minima of α-helical systems, respectively). As enumerated in Table 1, the CD data clearly indicate that the modification of histidine position results in only minor changes in the helical content of the bundle.

Peptide aggregation state

The association state of each of the variants, $[x10x24]_2$ (x = H or A) and $[HxA24]_2$ (x = 9–15), was evaluated using gel permeation chromatography (initial loading concentrations ranging from 0.1 to 100 μM) as shown for $[H14A24]_2$ in Figure 3. At all concentrations studied by gel permeation chromatography, the peptides elute with apparent molecular weights between 17.2 and 18.6 kDa (14.9–15.2 kDa calculated for the four helix bundles) based on a standardization curve derived from globular protein data as shown in Table 1. These peptides co-elute with the prototype $[H10H24]_2$, established to be a dimeric assembly by analytical ultracentrifugation, indicating that the related proteins have similar hydrodynamic radii, as expected. The data clearly demonstrate that these modifications result in no significant variation in the aggregation state preference of the bundle.

Thermodynamic stability

Disruption of the secondary and tertiary structure of each of the $[x10x24]_2$ (x = H or A) and $[HxA24]_2$ (x = 9–15) peptides was

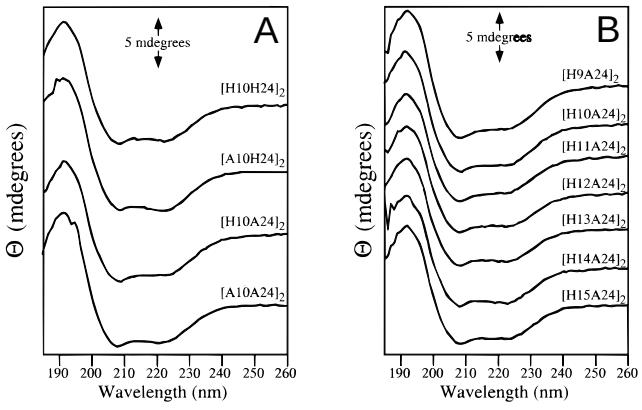

Fig. 2. Comparison of the far-UV CD spectra of the alanine variants of $[H10H24]_2$ recorded at 25 °C in 10 mM potassium phosphate, 100 mM KCl, pH 8.0 buffer. Peptide concentrations were 10 μM (2.5 μM four-helix bundle) as determined spectrophotometrically using Trp (ϵ_{280} = 5,600 M^{-1} cm^{-1} $helix^{-1}$).

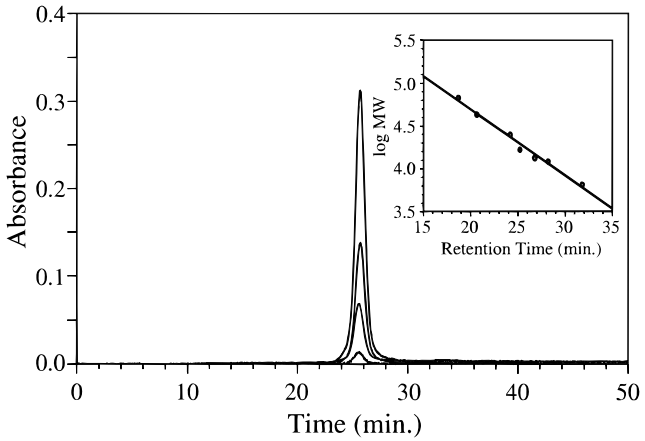

Fig. 3. Solution molecular weight determination of $[H14A24]_2$ via size-exclusion chromatography at initial loading concentrations (wavelength detected) of 100 μM (280 nm), 50 μM (280 nm), 500 nM (220 nm), and 100 nM (220 nm). Inset displays the column calibration curve used for interpolation of the peptide molecular weight, 17.6 amu. Experimental details are given in the text.

Table 2. *Thermodynamic evaluation of histidine variants at 25 °C*

Peptide	*m*	$[Gdn]_{1/2}$	ΔG^{H_2O} (25 °C)
$[H10H24]_2$	1.95	5.04	17.28
$[H10A24]_2$	3.12	5.59	24.88
$[A10H24]_2$	1.98	6.36	20.05
$[A10A24]_2$	2.55	6.26	23.39
$[H9A24]_2$	3.64	6.68	>30
$[H10A24]_2$	3.12	5.59	24.88
$[H11A24]_2$	—	7.53	—
$[H12A24]_2$	—	7.09	>25
$[H13A24]_2$	2.40	4.65	18.54
$[H14A24]_2$	2.44	4.99	19.59
$[H15A24]_2$	—	>8	—

accomplished by adding guanidine hydrochloride as the chaotrophic agent and observed by CD spectropolarimetry. At low concentrations of guanidine hydrochloride, the mean residue ellipticity at 222 nm ($[\Theta]_{222}$) is greater than $-25{,}000$ deg cm^2/dmol for all the peptides studied and thereby consistent with the designed high helical content. Figure 4 shows that upon addition of molar concentrations of guanidine hydrochloride $[\Theta]_{222}$ approaches zero indicating denaturation to form unordered structures. Six of the denaturation curves are sigmoidal with a single inflection point and a well-defined end point and, hence, consistent with a two-state equilibrium in which intermediates are minimally populated at equilibrium (Pace, 1986). The remaining four denaturation curves, data not shown, are not complete at the maximum 7.5 M guanidine hydrochloride allowing only estimation of the thermodynamic parameters. Table 2 shows that the midpoint of the denaturation curves ($[Gdn]_{1/2}$), molar cosolvation terms (m) and ΔG^{H_2O} values were highly dependent on the location of the histidines within the four helices for the peptide with well-defined end points. The pattern of global thermodynamic stabilities is consistent with the intended design.

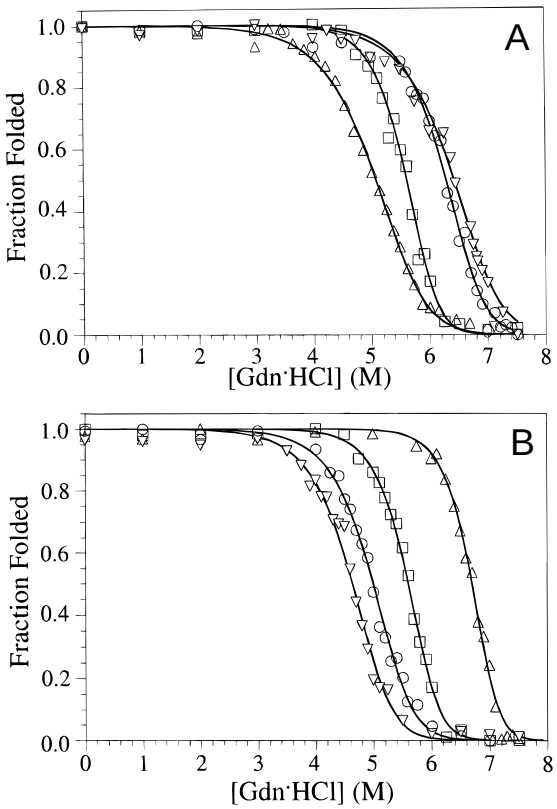

Fig. 4. Protein denaturation curves of each $[x10x24]_2$ (x = A or H) variant and each denaturable $[HxA24]_2$ (x = 9–15) variant peptide monitored by CD spectropolarimetry. **A:** $[H10H24]_2$ (△), $[H10A24]_2$ (□), $[A10H24]_2$ (▽), and $[A10A24]_2$ (○). **B:** $[H9A24]_2$ (△), $[H10A24]_2$ (□), $[H13A24]_2$ (▽), and $[H14A24]_2$ (○). For clarity, the curves for $[H11A24]_2$, $[H12A24]_2$, and $[H15A24]_2$, which did not have well-defined end points below 7 M Gdn, are not shown. All spectra were recorded at 25 °C in 10 mM potassium phosphate, 100 mM KCl, pH 8.0 buffer. Peptide concentrations were 3–10 μM as determined spectrophotometrically using Trp (ϵ_{280} = 5,600 M^{-1} cm^{-1}). The parameters used to fit each experimental curve are given in Table 2.

Ferric heme–peptide dissociation constants

The series of $[HxA24]_2$ (x = 9–15) peptides as well as $[A10A24]_2$ were screened for heme binding by addition of hemin to solutions of 100 μM peptide with overnight equilibration. The lack of observable spectral changes (to a red solution), relative to hemin in aqueous buffer (a green solution), placed a lower limit on the K_d value of ≈200 μM for $[A10A24]_2$, $[H9A24]_2$, and $[HxA24]_2$ (x = 12–15). Figure 5A shows a detailed examination for one of these, $[H9A24]_2$; the titration shows a linear increase in the absorbance at 412 nm with a slope equal to the molar absorptivity of free hemin in solution indicating the absence of oxidized heme binding to the histidine residues within the protein. These results are in sharp contrast with heme titrations of $[H10A24]_2$ and $[H11A24]_2$. Figure 5B describes the two independent K_d values for heme affinity $[H10A24]_2$ measured to be 15 and 800 nM. Figure 5C shows that $[H11A24]_2$ has a K_{d1} value of 9.5 μM; the binding of the second heme was too weak to be determined, which, under the limit of the measurements, indicated the K_{d2} value is >200 μM.

EPR of [H10A24]$_2$ and [H11A24]$_2$

The nature of the iron coordination and spin state of the ferric heme complexes of $[H10A24]_2$ and $[H11A24]_2$ was examined by cryogenic electron paramagnetic resonance (EPR) spectroscopy. Figure 6 shows that the EPR spectrum of $[H10A24]_2$ recorded at 20 K is clearly low-spin iron(III) with resonances at $g_{z,y,x}$ of 2.92, 2.27, and 1.51 values similar to those previously reported for $[H10H24]_2$ (Kalsbeck et al., 1996). A similar set of resonances is observed for $[H11A24]_2$, also supporting *bis*-histidine ligation; however, in this case there is a significant fraction of high spin iron(III) at g = 5.9 observed in the EPR spectrum as well. The lower affinity of $[H11A24]_2$ for heme most likely results in two ferric heme states: bound *bis*-histidine ligated ferric heme with low-spin EPR resonances, and unbound high-spin heme in a solution that yields the high-spin signal typical of free hemin. The rhombic and tetragonal splittings (Taylor, 1977), V/λ of 1.90 with D/λ of 3.18, calculated from the low-spin spectra of $[H10A24]_2$ and $[H11A24]_2$ are reminiscent of *bis*-imidazole ferric porphine

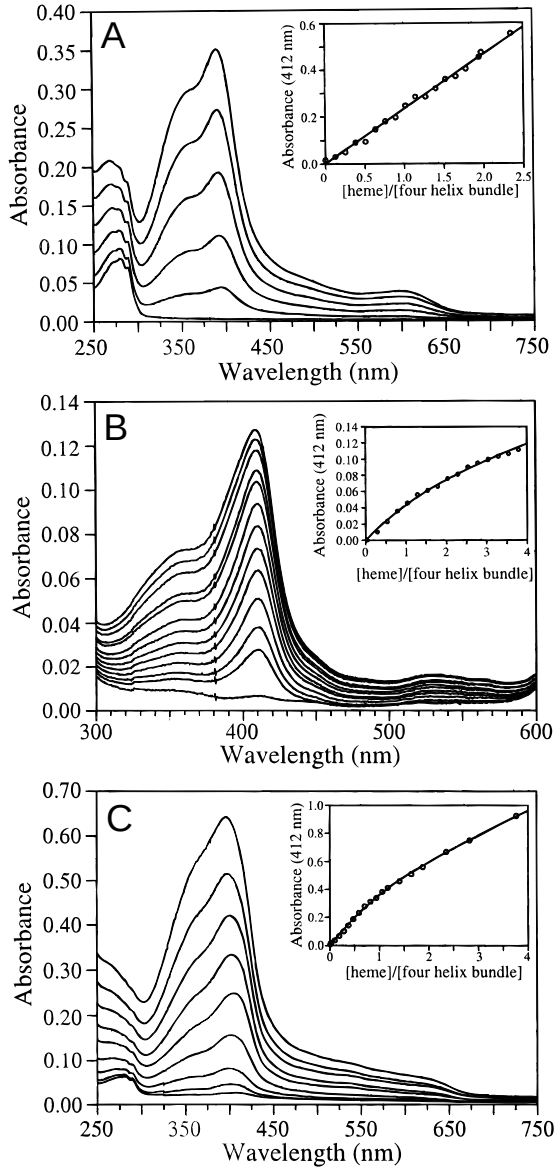

Fig. 5. Heme binding isotherms for $[H9A24]_2$, $[H10A24]_2$, and $[H11A24]_2$. **A:** Titration of hemin into a 31.2 μM $[H9A24]_2$ solution recorded in a 0.2 cm pathlength cuvette at 25 °C resulting in a green solution. Spectra shown contain 0.0, 0.13, 0.25, 0.38, 0.59, and 0.64 equivalents of added hemin per four helix bundle. **B:** Titration of hemin into a 54 nM $[H10A24]_2$ solution recorded in a 10 cm pathlength cuvette at 25 °C resulting in a red solution. Spectra shown contain 0.00, 0.38, 0.78, 1.16, 1.56, 1.96, 2.34, 2.74, 3.12, 3.62, 3.92, 4.30, and 4.70 equivalents of added hemin per four-helix bundle. **C:** Titration of hemin into a 21.2 μM $[H11A24]_2$ solution recorded in a 0.1 cm pathlength cuvette resulting in a red solution. Spectra shown contain 0.02, 0.0.094, 0.28, 0.47, 0.70, 0.94, 1.17, 1.64, and 2.35 equivalents of added hemin per the four-helix bundle. Insets display the absorbance at 412 nm vs. [heme]/[four helix bundle] ratio titration curve with fits. For clarity, the only the low [heme]/[four-helix bundle] ratio spectra are shown in **A** and **C**.

(1.94 and 3.12) and when plotted as rhombicity, V/D, vs. tetragonal crystal field, D/λ, both reside within the B group of heme EPR spectra of Peisach et al. (1973), indicating *bis*-histidine ligation to the ferric ions as designed (Walker et al., 1986).

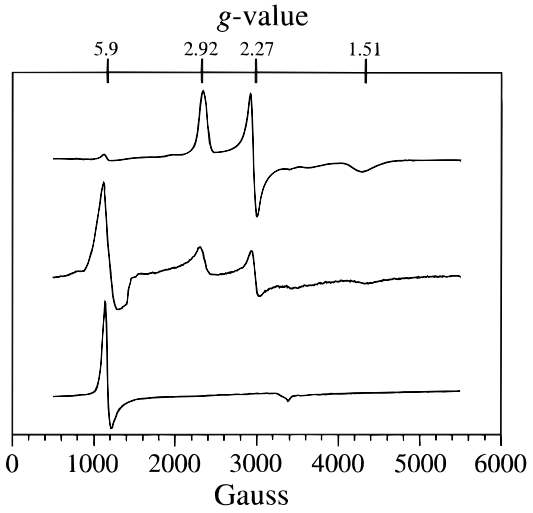

Fig. 6. Electron paramagnetic resonance characterization of the heme–protein maquettes. Frozen solution X-band EPR spectra of (top) *holo*-$[H10A24]_2$, (middle) *holo*-$[H11A24]_2$ (one heme per four-helix bundle). For comparison, the EPR spectrum of (bottom) heme-BSA is shown. EPR spectral acquisition parameters are given in the text.

Heme redox potentiometry

The electrochemical redox potential of the single bound heme in *holo*-$[H11A24]_2$ was determined by monitoring the changes in the α- and β-bands of the absorption spectra as a function of redox potential. Figure 7 shows a redox titration of *holo*-$[H11A24]_2$ fit to a single $n = 1$ Nernst curve with a midpoint (E_{m8}) of -166 ± 10 mV. The midpoint potential of the heme in *holo*-$[H11A24]_2$ is quite similar to the value for a single heme in [H10A24] (E_{m8} of -155 mV) (Shifman et al., 1998) and distinctly lower than that observed for a single heme in *holo*-$[A10H24]_2$, E_{m8} of -110 mV (B.R. Gibney, unpubl. obs.). The data indicate that the hemes of

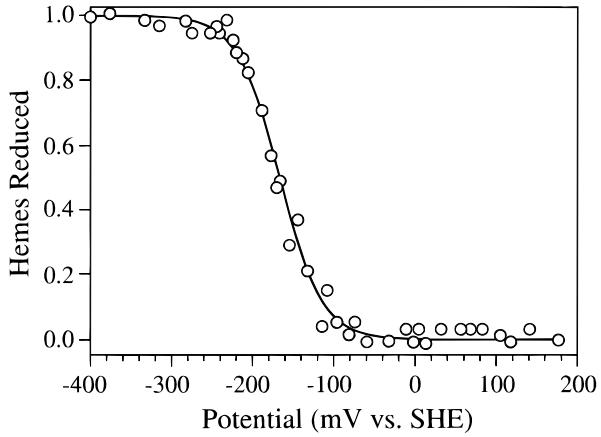

Fig. 7. Redox titration curve of *holo*-$[H11A24]_2$ monitored by optical spectroscopy at 25 °C. The number of hemes reduced was determined by the change in absorbance at 559 nm (α-band maximum) relative to baseline absorbance (760 nm) normalized to four hemes for the entire titration. The experimental data points were fit to the single Nernst equation curve ($n = 1$ fixed).

$[H10A24]_2$ and $[H11A24]_2$ reside in similar electrochemical environments, whereas the heme in $[A10H24]_2$ is easier to reduce due to the electrostatic interaction with the positively charged arginine residues at position 27.

Discussion

Using the prototype heme protein maquette, we have investigated the role of histidine ligand placement on heme affinity in a highly helical, water soluble, and stable four-α-helix bundle scaffold. The heme–protein dissociation constants for $[H10A24]_2$ and $[A10H24]_2$, formed by removal of two $[H10H24]_2$ heme binding sites by substituting alanine residues for histidines, indicate that the placement of the heptad **a**–heptad **a bis**-histidine binding site near the N-terminus is preferred by 2.3 kcal/mol in this peptide architecture. Due to this higher thermodynamic affinity of $[H10A24]_2$ for hemes, it was selected as the template for a systematic study the effect of the relative placement of histidine residues on heme binding. A series of seven peptides, representing the rotation of histidine through a continuous heptad, demonstrates rigid design specifications for heme binding with narrow tolerances.

Tables 1 and 2 illustrate the inherent robustness and invariability of the four-α-helix scaffold architecture for the construction of maquettes. The proteins studied represent very stable maquette scaffolds, most likely is due to the length and the relatively high hydrophobic content of their helices, which has facilitated their incorporation into self-assembled monolayer and Langmuir–Blodgett films for material science applications such as biochemical sensors (Chen et al., 1998; Pilloud et al., 1998). The global stability of the protein allows for local modification of the amino acid composition without significant changes in aggregation state or helical content, illustrating the validity of using this maquette scaffold for investigations of optimal heme ligand placement. It is clear that the replacement of bulky, polar hydrophilic histidine residues within the hydrophobic core with small apolar hydrophobic alanines results in enhanced global peptide stability. However, the magnitude of stabilization is highly context dependent in this anisotropic protein matrix, as $[H10A24]_2$ and $[A10H24]_2$ have identical amino acid composition but differ by nearly 5 kcal/mol in their global stabilities. The lower stability of $[A10H24]_2$ and $[A10A24]_2$ compared to $[H10A24]_2$ suggests the alanine may be too small a hydrophobic residue for position 10, leaving a small cavity or cleft that replacement with a bulkier histidine may serve to fill, more than compensating for the expected destabilization due to insertion of a polar residue into the hydrophobic core.

The proper location of the designed interior heptad positions is illustrated by tracking the substitution of histidine residues through a continuous heptad, the $[HxA24]_2$ (x = 9–15) variants. Heptad positions **a** ($[H10A24]_2$), **d** ($[H13A24]_2$), and **e** ($[H14A24]_2$) show reduced global peptide stability due the replacement of hydrophobic residues with a polar side chain. Unfortunately, the placement of a histidine residue on the peptide exterior, $[H9A24]_2$ (heptad position **g**), $[H11A24]_2$ (**b**), $[H12A24]_2$ (**c**), and $[H15A24]_2$ (**f**), yields peptides whose thermodynamic stability is too high to be accurately assessed. Because these peptides are variants of $[A10A24]_2$ with the hydrophilic residues glutamate and lysine substituted with histidine, it is not clear as to the source of their enhanced thermodynamic stabilities that exceed that of the parent peptide. In the absence of detailed structural information on these peptides, it is hard to definitively ascertain the molecular basis for their marked increase in stability relative to $[A10A24]_2$.

Evaluation of the heme–protein dissociation constants demonstrates a modulation of the heme affinity by the histidine residue location within the different heptads of the protein. Clearly, the removal of pairs of histidines in the conceptual progression from $[H10H24]_2$ through $[H10A24]_2$ and $[A10H24]_2$ to $[A10A24]_2$ reduces the heme–protein stoichiometry, illustrating the necessity of the histidine ligands for heme binding in these peptides. Of the peptides studied with designed heptad **a**–heptad **a** heme binding sites, position 10 of $[H10A24]_2$ has the greatest affinity, K_{d1} of 15 nM. The heme affinity of $[A10H24]_2$ displays a K_{d1} of 800 nM, some 50-fold weaker but still appreciable. Obviously, the folding of the protein into a defined architecture places the histidine ligands in close proximity forming a heme binding site, thus negating the energetic cost of binding the iron in a chelate ring of 68 atoms (H10,H10′) or 125 atoms (H24,H24′). The distinct heme affinities of $[H10A24]_2$ and $[A10H24]_2$ (K_{d1} values of 15 and 800 nM, respectively) represent an energetic difference of about 2.3 kcal/mol. This disparity in the heme binding energy may reflect electrostatic differences in the local vicinity of the hemes. The 2.3 kcal/mol lower affinity in $[A10H24]_2$ compared to $[H10A24]_2$ is due in part to the interaction of the oxidized heme (+1 formal charge) and the charged arginine residues at position 27 (heptad **d**), because the 45 mV E_{m8} difference, respective E_{m8} values of −110 and −155 mV, accounts for 5.5-fold (1 kcal/mol) of the K_{d1} difference. The two analogous hemes in the cytochrome bc_1 complex, b_L and b_H, have potentials of −90 mV and +50 mV (Dutton et al., 1970; Dutton & Jackson, 1972), an E_{m8} difference of 140 mV, due in part to arginine residues local to the b_H site. Electrostatic stabilization of ferric heme binding by via an ion pair between the propionates (−) and arginine residues (+), as observed in myoglobin (Hunter et al., 1997), or charge compensation local to the heme iron provides an additional design concept for the next generation of designed heme proteins.

Figure 8 illustrates that permutation of the histidine residues through a continuous heptad shows a high sensitivity of the heme affinity to the heptad position of the ligand residues. Evaluation of

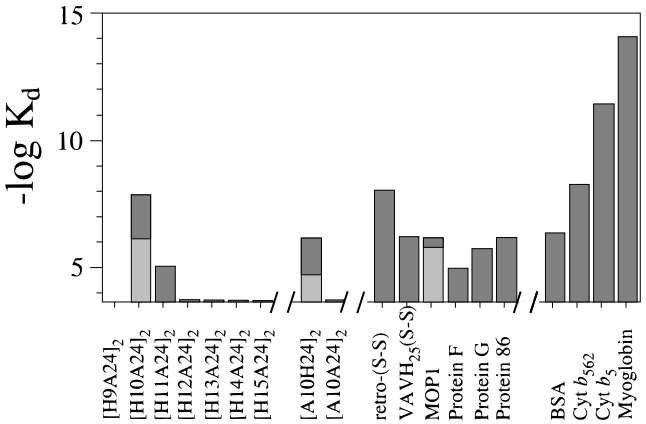

Fig. 8. Representation of the oxidized heme affinity parameter through a heptad repeat of $[H10A24]_2$ and comparison with several designed and natural heme proteins. The designed proteins include DeGrado's Retro(S-S) and VAVH(S-S), Haenel's MOP1 and Hecht's Proteins F, G, and 86. The heme affinity is given as the $\log K_d$ value with the first heme binding constant in black and the second represented in gray where appropriate. The lower limit of the graph (*) represents the 200 μM detection limit in the heme binding assay.

the heme–protein dissociation constants demonstrates that only $[H10A24]_2$ (heptad **a**–heptad **a**) and $[H11A24]_2$ (heptad **b**–heptad **b**) bind heme with K_{d1} values tighter than 100 μM. Although $[H10A24]_2$ ligates a pair of hemes with high affinity (K_{d1} of 15 nM and K_{d2} of 800 nM), $[H11A24]_2$ only binds a single heme per the four-α-helix bundle (two potential heme binding sites) with 800-fold (3.9 kcal/mol) lower affinity, K_{d1} of 9.5 μM. The remainder of this peptide series do not bind hemes with a K_{d1} tighter than $<$200 μM, indicating that the heme–protein interaction energy has dropped by $>$5 kcal/mol by moving the histidine ligands—even in the case where the histidines are only moved a single heptad position, i.e., $[H9A24]_2$. The precipitous drop in heme affinity between $[H10A24]_2$ and $[H9A24]_2$ illustrates the demanding engineering tolerances within this highly stable maquette scaffold. Based on a helical wheel diagram of an all-parallel four-stranded coiled-coil protein (Fig. 1), it is reasonable to expect that $[H13A24]_2$ (heptad **d**–heptad **d**) and $[H14A24]_2$ (heptad **e**–heptad **e**) might posses moderate heme affinity. The formation of a $[H13A24]_2$ and $[H14A24]_2$ *bis*-histidine binding site appears to require only slight rotation of the helices, whereas the formation of the observed $[H11A24]_2$ heme binding site (heptad **b**–heptad **b**) appears to require significant helix rotation/deformation that may be part of 3.9 kcal/mol lower heme–protein interaction relative to $[H10A24]_2$. However, the $[H13A24]_2$ and $[H14A24]_2$ site may also have lowered heme affinity due to steric interactions with the phenylalanines at position 17, the center of the designed helix and presumably the crossover point of the two di-α-helical monomers. The tight packing of the hydrophobic core near the center of the helices coupled with the high protein stability may prevent the incorporation of the heme macrocycle despite a thermodynamically favorable ligand set.

A benchmark to differentiate adventitious heme binding and heme binding to a designed site is provided by the heme affinity for "off-the-shelf" proteins such as bovine serum albumin (BSA) and human serum albumin (HSA) (Hollfelder et al., 1996). Heme binds to serum albumins at multiple locations with the tightest site having a dissociation constant of 0.5 μM (Beaven et al., 1973) and possessing EPR spectral properties characteristic of a high spin heme as shown in Figure 6 (Bearden et al., 1974). The 9.5 μM dissociation constant for the first, low-spin, heme of $[H11A24]_2$ is about 20-fold weaker than BSA and quite similar to that measured for the denatured state of cytochrome b_{562} (K_d value of 3 μM) (Robinson et al., 1997), indicating that $[H11A24]_2$ is well within the realm of adventitious heme binding. In stark contrast, $[H10A24]_2$ binds heme significantly tighter (4.8 kcal/mol; 3,000-fold) than BSA and at precisely the designed stoichiometry. The K_{d1} value observed for $[H10A24]_2$ lies between the native state low-spin *bis*-histidine ligated *b*-type cytochrome b_5 (4 pM) (Gruenke et al., 1997) and the histidine–methionine ligated cytochrome b_{562} (6 nM) (Robinson et al., 1997). However, the heme–protein interaction in the tightest binding site of $[H10A24]_2$ is still 4.8 kcal/mol less favorable than cytochrome b_5. Furthermore, these heme protein K_d values are three to five orders of magnitude weaker than myoglobin (Hargrove et al., 1996) revealing the inadequacies of the current designs, which to date do not possess a designed heme pocket.

With the potential evaluation of $[H11A24]_2$ as an adventitious heme binding protein, the electrochemistry of the bound heme might be expected to resemble either *bis*-imidazole iron protoporphyrin IX, $Fe(PPIX)(Im)_2$, in aqueous solution or perhaps heme bound to BSA. The midpoint potential of the heme complex of $[H11A24]_2$ is -166 mV (Fig. 7), a value some 150 mV (Shifman et al., 1998) more positive than $Fe(PPIX)(Im)_2$, and approaching the -104 mV (Rivera et al., 1994) value observed for rat liver microsomal cytochrome b_5 (Table 3), illustrating that it does not resemble $Fe(PPIX)(Im)_2$. Additionally, the midpoint potential of the heme bound to $[H11A24]_2$ is slightly higher than that of heme bound to BSA, $E_{m8} = -190$ mV (data not shown), and the EPR spectra are distinct demonstrating the differences between these adventitious heme binding proteins. Furthermore, the midpoint potential of $[H10A24]_2$ containing only one heme is nearly identical to *holo*-$[H11A24]_2$ at -155 mV, indicating that the irons of *holo*-$[H11A24]_2$ and singly occupied *holo*-$[H10A24]_2$ reside in similar electrochemical environments. The elevation of the midpoint potentials of $[H11A24]_2$ and $[H10A24]_2$, relative to $Fe(PPIX)(Im)_2$ and heme-BSA, is due to the ligation of the iron and sequestration from the bulk solvent (Stellwagen, 1978), with the further elevation of the heme midpoint potential in $[A10H24]_2$ attributable to local electrostatic effects. The similar modulation of the heme reduction potential observed upon binding of the iron and insertion of the heme macrocycle within the low dielectric protein interior in $[H11A24]_2$ and $[H10A24]_2$ demonstrates that the ratio of the oxidized to reduced heme dissociation constants is equivalent. This suggests that the differences in K_{d1} values between

Table 3. *Comparison of designed heme protein properties*

Peptide	*bis*-Histidine ligation motif	K_d	E_m
Cytochrome b_5	NA	4 pM	-104 mV
$[H10A24]_2$	heptad **a**–heptad **a**	15 nM, 800 nM	-170, -265 mV
$[A10H24]_2$	heptad **a**–heptad **a**	800 nM, 20 μM	-75, -205 mV
$[H11A24]_2$	heptad **b**–heptad **b**	9.5 μM	-166 mV
retro-(S-S)	heptad **d**–heptad **d**	10 nM	-220 mV
$VAVH_{25}$(S-S)	heptad **d**–heptad **d**	700 nM	-170 mV
MOP1	heptad **a**–heptad **a**	$<$1 μM	-110, -170 mV
Protein 86	heptad **b**–heptad **f**[a]	740 nM	ND
Protein F	heptad **b**–heptad **b**[a]	12 μM	ND
Protein G	heptad **c**–heptad **X**[a]	2 μM	ND

[a]These are proposed ligation motifs, other combinations are also possible.

$[H10A24]_2$ and $[H11A24]_2$ are due to local structural changes upon porphyrin macrocycle incorporation rather than due to burial of the charged ferric porphyrin, which is equally difficult in both cases. Additionally, as already mentioned, the weaker heme–protein affinity of $[A10H24]_2$ and higher midpoint potential can be ascribed to repulsive interactions between the ferric heme and the arginine residues in the next hydrophobic packing layer because the ratio of the oxidized-to-reduced heme dissociation constants is altered in this protein relative to $[H10A24]_2$.

A protein design rule evident from the data presented is that a *bis*-histidine binding site composed of two heptad **a** positions is favored within the particular maquette scaffold chosen, a homotetrameric helical bundle. Coupled with other examples of successful heme protein design based on four-α-helix bundles with histidine ligation, a more general picture of heme binding in synthetic peptides may be developed. For example, retro(S-S) (Choma et al., 1994) with an estimated K_d value of 10 nM and reduction potential, E_{m8}, of -220 mV, utilizes a heme site composed of a pair of histidines in heptad **d** positions that are diagonally disposed across the interior of a four helix bundle. In comparison to $[H13A24]_2$, incompetent to bind heme but with similar histidine ligand placement, the success of retro(S-S) demonstrates that hydrophobic packing plays an important role in determining the affinity for incorporation of the porphyrin macrocycle. Additionally, a template assisted synthetic peptide (MOP1) (Rau & Haehnel, 1998), based on cytochrome bc_1 complex and similar to $[H10H24]_2$, employs two heptad **a** to heptad **a** *bis*-histidine ligation sites diagonally across the hydrophobic core. Although precise heme–protein K_d values were not reported for MOP1, both can be conservatively estimated at <1 μM. Therefore, tight heme binding can be achieved with *bis*-hisitidine ligation from heptad **a**–heptad **a** or with heptad **d**–heptad **d** ligation with hydrophobic packing modulating macrocycle affinity. Additionally, as in $[H11A24]_2$, moderate heme affinity can be achieved with heptad **b**–heptad **b** **bis**-histidine ligation in the absence of a designed cavity.

The heme protein design specifications delineated from designed proteins with established ligation motifs may be applied to four-α-helix heme proteins selected from combinatorial libraries. By comparison to the successful designed proteins, it is possible to suggest likely heme ligation motifs, based on heme–ligand affinity, in the combinatorial library of Hecht and coworkers (Rojas et al., 1997), whose heme–ligand identities and relative placement in the protein have not been ascertained with any degree of certainty. Heme binding affinity similar to the *bis*-histidine ligated $[H11A24]_2$ (heptad **b**–heptad **b**) protein is observed for Protein F (K_d of 4 μM), where a *bis*-histidine site from His43 (heptad **b** on helix II) to His69 (heptad **b** on helix IV) is one of several possible ligand combinations. Protein 86 (K_d value of 740 nM) has heme optical spectra in the reduced state typical of *bis*-histidine ligation, suggesting it may be bound by a *bis*-histidine site formed between His31 (heptad **b** on helix II) and His73 (heptad **f** helix IV). The only other protein from the library with a quantitated heme affinity, Protein G (K_d of 35 μM, well above the adventitious heme affinity threshold), must have at least one heptad **c** position histidine for *bis*-histidine ligation that may be permissible in this less stable protein scaffold. Additionally, two peptides in the library that bind oxidized heme, Z and 24, contain all of the histidine ligands on a single helix, implying that *bis*-histidine heme binding may involve four-α-helix bundle dimerization, akin to that observed in cytochrome b_1 (bacterioferritin) (Frolow et al., 1994), where the *bis*-methionine ligation is provided from a dimer of four-α-helix bundles; this situation is possible but not observed for the $[H12A24]_2$ or $[H15A24]_2$ peptides.

It is evident that the protein design rules derived from this study are applicable for evaluating the results of randomized combinatorial libraries as well as improving future heme protein designs. Additionally, these design rules may also be implemented into automated protein design strategies (Hellinga & Richards, 1991; Desjarlais & Handel, 1995; Dahiyat & Mayo, 1997; Lazar et al., 1997). Although it is well recognized that heme affinity is the result of numerous factors within natural proteins, herein we have attempted to solely address the role of ligand placement, which should directly influence the ligand–metal bond strength and heme affinity. Future designs may modify the potential heme macrocycle–hydrophobic residue interactions that are demonstratively critical to successful heme protein design. These types of indirect interactions may serve in future designs to stabilize the heme peptides to allow for the loss of a heme ligand, generating a five coordinate heme with potential chemical reactivity.

Materials and methods

Materials

Trifluoroacetic acid, diethyl ether, acetic anhydride, piperidine, and pyridine were obtained from the Aldrich Chemical Company (Milwaukee, Wisconsin). Ethanedithiol and 1-hydroxybenzotriazole (HOBt) were purchased from Fluka (Buchs, Switzerland). Fmoc-protected amino acids were secured as pentafluorophenyl esters from PerSeptive Biosystems (Framingham, Massachusetts, with the exception of Fmoc-L-Arg(Pmc)-OPfp, which was purchased from Bachem (King of Prussia, Pennsylvania). NovaSyn PR-500 resin was obtained from Calbiochem-Novabiochem (San Diego, California). Guanidine hydrochloride (8 M) was used as received from Pierce (Rockford, Illinois). All other chemicals and solvents were reagent grade.

Methods

Preparation of peptides: General procedure

The peptides were synthesized on a continuous flow PerSeptive Biosystems Pioneer solid-phase synthesizer using the Fmoc/^{t}Bu protection strategy (Bodanszky, 1993) with NovaSyn PR-500 resin (0.33 mmol/g loading) at 0.2 mmol scale. Single coupling cycles (30 min) with OPfp/HOBt chemistry were employed for all amino acids. The side-chain protecting groups used are as follows: Lys (^{t}Boc); Glu (O^{t}Bu); Cys (Trt); His (^{t}Boc); Arg (Pmc). To stabilize helix formation, terminal charges were neutralized by amidation of the C-termini and manual acetylation of the N-termini of the peptides. Following chain assembly and acetylation, the peptide resins were thoroughly washed with DMF and CH_2Cl_2 before cleavage from the resin and simultaneous side-chain deprotection using 90:8:2 (v/v/v) trifluoroacetic acid (TFA):ethanedithiol:water for 2 h. After washing the resin with neat TFA, the filtrate was concentrated by evaporation with a flow of dry argon, and the crude peptides were precipitated and washed with cold ether, dissolved in water (0.1% v/v TFA), and lyophilized to dryness. The peptides were purified to homogeneity by reversed-phase C_{18} high-performance liquid chromatography (HPLC) (Vydac C_{18} column) using aqueous-

acetonitrile gradients containing 0.1% (v/v) TFA. The N-terminal cysteine residues of the purified peptides were air oxidized to the symmetric disulfides in 100 mM ammonium carbonate buffer, pH 9.5 (5 h). The dimerization process was followed by analytical HPLC. After lyophilization, the identities and purities of the resulting disulfide bridged di-α-helical peptides, (α-SS-α), were confirmed with laser desorption mass spectrometry and reversed-phase-HPLC, respectively.

Solution molecular weight determination

Size-exclusion chromatography was performed using a Beckman System Gold HPLC pump equipped with a diode array detector coupled to a Pharmacia FPLC Superdex 75 column eluted with aqueous buffer (10 mM KP_i, 100 mM KCl, pH 8.0) at a flow rate of 0.5 mL/min. The column was standardized using aprotinin (6.5 kDa), horse heart cytochrome *c* (12.1 kDa), ribonuclease A (13.4 kDa), myoglobin (16.7 kDa), chymotrypsinogen (25.0 kDa), ovalbumin (43.0 kDa), and bovine serum albumin (67.0 kDa). The eluents were monitored at 220 nm and solution molecular weights determined by interpolation.

CD spectropolarimetry

CD spectra were recorded on an AVIV 62DS spectropolarimeter using rectangular quartz cells of a 0.2 cm pathlength with a 10 s averaging time. Thermal control was maintained by a thermoelectric module with a Neslab CFT-33 refrigerated recirculating water bath as a heat sink. Peptide concentrations were between 2.5–3.0 μM (four helix bundle) as determined spectrophotometrically using $\epsilon_{280} = 5{,}600\ M^{-1}\ cm^{-1}\ helix^{-1}$ for Trp.

Denaturation studies

Peptide denaturation curves at 25 °C were fit to a dimer folded to two monomer unfolded equilibrium (Mok et al., 1996) using a nonlinear least-squares routine in KaleidaGraph (Abelbeck Software, Reading, Pennsylvania) to the following equation:

$$\text{fraction folded} = 1 - (\exp(-\Delta G_{unf}/RT)/4P) \times [(1 + 8P/\exp(-\Delta G_{unf}/RT))^{1/2} - 1]$$

where P is the molar concentration of total monomeric protein and $\Delta G_{unf} = \Delta G^{H_2O}$-$m$[Gdn·HCl], m is the cosolvation term, which is a measure of the cooperativity of the transition, and [denaturant] is the concentration of denaturant (M).

UV-VIS spectroscopy

UV-visible spectra were recorded on a Perkin-Elmer (Foster City, California) Lambda 2 spectrophotometer using quartz cells of 0.1-, 0.2-, 1.0-, and 10-cm pathlength. Peptide concentrations were determined spectrophotometrically using $\epsilon_{280} = 5{,}600\ M^{-1}\ cm^{-1}$ for tryptophan.

Heme incorporation

A DMSO solution of hemin was added in 0.1 equivalent aliquots to peptide solutions (10 mM KP_i, 100 mM KCl, pH 8.0) with 10 min equilibration between additions. The K_d values were obtained from the absorbance at 412 nm plotted against [heme]/[four-helix bundle] according to an equation for two independent binding sites (Price & Dwek, 1979).

Purification of holo peptide

Preparative size-exclusion chromatography was performed using a Pharmacia (Uppsala, Sweden) FPLC High-Load 16/60 Superdex 75 prep grade column interfaced with a Beckman (Fullerton, California) System Gold HPLC system pump with a diode array detector eluted with aqueous buffer (10 mM KP_i, 100 mM KCl, pH 8.0) at a 2 mL/min flow rate. The sample provided a chromatogram consistent with that obtained from the analytical size-exclusion column. The four-helix bundle fraction was collected and concentrated in Centriprep-3 centrifugal force concentrators in a Beckman J-21C centrifuge. Analytical size-exclusion chromatography of the concentrated peptide displayed a single species of molecular weight consistent with a four-helix bundle aggregation state.

EPR spectroscopy

Electron paramagnetic resonance (EPR) spectroscopy was performed using a Bruker (Karlsruhe, Germany) ESP300E spectrometer with temperature control maintained by an Oxford ESR 900 continuous-flow liquid helium cryostat interfaced with an Oxford ITC4 temperature controller. Frequency was measured by a Hewlett-Packard 5350B frequency counter. Typical EPR parameters: sample temperature, 20 K; microwave frequency, 9.447 GHz; microwave power, 5 mW; modulation frequency, 100 kHz; modulation amplitude, 20.0 G; time constant, 164 ms; number of scans, 5.

Redox potentiometry

Chemical redox titrations (Dutton, 1978) were performed in an anaerobic cuvette equipped with a platinum working and a calomel reference electrode. Ambient redox potentials (measured against the standard hydrogen electrode) were adjusted by addition of aliquots (<1 μL) of sodium dithionite or potassium ferricyanide. Titrations were performed in 10 mM potassium phosphate, 100 mM KCl, pH 8.0. Electrode-solution mediation was facilitated by the following mediators at 10 μM concentration: benzyl viologen, 2-hydroxy-1,4-naphthoquinone, anthroquinone-2-sulfonate, duroquinone, phenazine ethosulfate, phenazine methosulfate, 1,4-benzoquinone, 1,2-naphthoquinone, and 1,4-naphthoquinone. After equilibration at each potential, the optical spectrum was recorded. Reduction of the heme in $[H11A24]_2$ was followed by the increase in the α-band absorption at 559 nm. Spectral intensity was plotted against potential and the data were fit to a single Nernst equations with $n = 1.0$ (fixed).

Acknowledgments

This work was supported by a National Institutes of Health grant to P.L.D. (GM 41048) in part by the MRSEC Program of the NSF under award DMR96-32598, and an NSRA postdoctoral grant to B.R.G. (GM 17816). The authors thank Ms. Julie Baker for aid in the synthesis of $[A10A24]_2$. Mass spectroscopic analyses were performed by the Protein Chemistry Laboratory of the University of Pennsylvania.

References

Arnold PA, Benson DR, Brink DJ, Hendrich MP, Jas GS, Kennedy ML, Petasis DT, Wang MX. 1997a. Helix induction and springboard strain in peptide-sandwiched mesohemes. *Inorg Chem 36*:5306–5315.

Arnold PA, Shelton WR, Benson DR. 1997b. Peptide helix induction in a self-assembling hemoprotein model. *J Am Chem Soc 119*:3181–3182.

Bearden AJ, Morgan WT, Muller-Eberhard U. 1974. Heme complexes of rabbit hemoplexin, human hemoplexin and human serum albumin: Electron spin resonance and Mossbauer spectroscopic studies. *Biochim Biophys Res Commun 61*:265–272.

Beaven GH, Chen SH, D'Albis A, Gratzer WB. 1973. A spectroscopic study of the haemin–human–serum–albumin system. *Eur J Biochem 41*:539–546.

Benson DE, Wisz MS, Liu WT, Hellinga HW. 1998. Construction of a novel redox protein by rational design: Conversion of a disulfide bridge into a mononuclear iron-sulfur center. *Biochemistry 37*:7070–7076.

Benson DR, Hart BR, Zhu X, Doughty MB. 1995. Design, synthesis, and circular-dichroism investigation of a peptide-sandwiched mesoheme. *J Am Chem Soc 117*:8502–8510.

Bodanszky M. 1993. *Peptide chemistry: A practical approach*, 2nd ed. New York: Springer Verlag.

Bryson JW, Betz SF, Lu HS, Suich DJ, Zhou HX, O'Neil KT, DeGrado WF. 1995. Protein design—A hierarchical approach. *Science 270*:935–941.

Bryson JW, Desjarlais JM, Handel TM, DeGrado WF. 1998. From coiled coils to small globular proteins: Design of a native-like three-helix bundle. *Protein Sci 7*:1404–1414.

Chen X, Moser CC, Pilloud DL, Dutton PL. 1998. Molecular orientation of Langmuir-Blodgett films of designed heme protein and lipoprotein maquettes. *J Phys Chem B 102*:6425–6432.

Choma CT, Lear JT, Nelson MJ, Dutton PL, Robertson DE, DeGrado WF. 1994. Design of a heme-binding 4-helix bundle. *J Am Chem Soc 116*:856–865.

Crick FHC. 1953. The packing of alpha helices: Simple coiled coils. *Acta Crystallogr 6*:689–697.

Dahiyat BI, Mayo SL. 1997. De novo protein design: Fully automated sequence selection. *Science 278*:82–87.

D'Auria G, Maglio O, Nastri F, Lombardi A, Morelli G, Paolillo L, Pedone C, Pavone V. 1997. Hemoprotein models based on a covalent helix-heme-helix sandwich. 2. Structural characterization of Co-III mimochrome I Delta and Delta isomers. *Chem Eur J 3*:350–362.

deMaré F, Kurtz DMJ, Nordlund P. 1996. The structure of *Desulfovibrio vulgaris* rubrerythrin reveals a unique combination of rubredoxin-like FeS_4 and ferritin-like diiron domains. *Nat Struct Biol 3*:539–546.

Desjarlais JM, Handel TM. 1995. De novo design of the hydrophobic cores of proteins. *Protein Sci 4*:2006–2018.

Dieckmann GD, McRorie DK, Lear JD, Sharp KA, DeGrado WF, Pecoraro VL. 1998. The role of protonation and metal chelation preferences in defining the properties of mercury-binding coiled coils. *J Mol Biol 280*:897–912.

Dieckmann GD, McRorie DK, Tierney DL, Utschig LM, Singer CP, O'Halloran TV, Penner-Hahn JE, DeGrado WF, Pecoraro VL. 1997. De novo design of mercury-binding two- and three-helical bundles. *J Am Chem Soc 119*:6195–6196.

Ding H, Moser CC, Robertson DE, Tokito MK, Daldal F, Dutton PL. 1995. Ubiquinone pair in the Q_o site central to the primary energy conversion reactions of cytochrome bc_1 complex. *Biochemistry 34*:15979–15996.

Dolphin GT, Brive L, Johansson G, Baltzer L. 1996. Use of aromatic amino acid residues to restrict the dynamics in the hydrophobic core of a designed helix-loop-helix dimer. *J Am Chem Soc 118*:11297–11298.

Dutton PL. 1978. Redox potentiometry: Determination of midpoint potentials of oxidation-reduction components of biological electron-transfer systems. *Methods Enzymol 54*:411–435.

Dutton PL, Jackson JB. 1972. Thermodynamic and kinetic characterization of electron transfer components in situ in *Rhodopseudomonas spheroides* and *Rhodospirillum rubrum*. *Eur J Biochem 39*:495–510.

Dutton PL, Wilson DF, Lee CP. 1970. Oxidation-reduction potentials of cytochromes in mitochondria. *Biochemistry 9*:5077–5082.

Farinas E, Regan L. 1998. The de novo design of a rubredoxin-like Fe site. *Protein Sci 7*:1939–1946.

Finzel BC, Weber PC, Hardman KD, Salemme FR. 1985. Structure of ferricytochrome c' from *Rhodospirillum molischianum* at 1.67 A resolution. *J Mol Biol 186*:627–643.

Frolow F, Kalb AJ, Yariv J. 1994. Structure of a unique twofold symmetrical heme-binding site. *Nat Struct Biol 1*:453–460.

Ghadiri MR, Choi C. 1990. Secondary structure nucleation in peptides—Transition-metal ion stabilized alpha-helices. *J Am Chem Soc 112*:1630–1632.

Gibney BR, Johansson JS, Rabanal F, Skalicky JJ, Wand AJ, Dutton PL. 1997a. Global topology & stability and local structure & dynamics in a synthetic spin-labeled four-helix bundle protein. *Biochemistry 36*:2798–2806.

Gibney BR, Mulholland SE, Rabanal F, Dutton PL. 1996. Ferredoxin and ferredoxin-heme maquettes. *Proc Natl Acad Sci USA 93*:15041–15046.

Gibney BR, Rabanal F, Dutton PL. 1997b. Synthesis of novel proteins. *Curr Opin Chem Biol 1*:537–542.

Gibney BR, Rabanal F, Reddy KS, Dutton PL. 1998. Effect of four helix bundle topology on heme binding and redox properties. *Biochemistry 37*:4635–4643.

Gibney BR, Rabanal F, Skalicky JJ, Wand AJ, Dutton PL. 1997c. Design of a unique protein scaffold for maquettes. *J Am Chem Soc 119*:2323–2324.

Gibney BR, Rabanal F, Skalicky JJ, Wand AJ, Dutton PL. 1999. Iterative protein redesign. *J Am Chem Soc 121*:4952–4960.

Gruenke LD, Sun, J, Loehr TM, Waskell L. 1997. Resonance Raman spectral properties and stability of manganese protoporphyrin IX cytochrome b_5. *Biochemistry 36*:7114–7125.

Hargrove MS, Barrick D, Olson JS. 1996. The association rate constant for heme binding to globin is independent of protein structure. *Biochemistry 35*:11293–11299.

Hayashi O. 1962. *Oxidases*. New York: Academic Press.

Hellinga HW. 1998a. Construction of a blue copper analogue through iterative rational protein design cycles demonstrates principles of molecular recognition in metal center formation. *J Am Chem Soc 120*:10055–10066.

Hellinga HW. 1998b. The construction of metal centers in proteins by rational design. *Folding Design 3*:R1–R8.

Hellinga HW, Richards FM. 1991. Construction of new ligand-binding sites in proteins of known structure. 1. Computer-aided modeling of sites with predefined geometry. *J Mol Biol 222*:763–785.

Hill RB, DeGrado WF. 1998. Solution structure of α_2D, a nativelike de novo designed protein. *J Am Chem Soc 120*:1138–1145.

Hollfelder F, Kirby AJ, Tawfik DS. 1996. Off-the-shelf proteins that rival tailor-made antibodies as catalysts. *Nature 383*:60–63.

Hunter CL, Lloyd E, Eltis LD, Rafferty SP, Lee H, Smith M, Mauk AG. 1997. Role of the heme propionates in the interaction of heme with apomyoglobin and apocytochrome b_5. *Biochemistry 36*:1010–1017.

IUBAB. 1992. *Enzyme nomenclature 1992*. San Diego: Academic Press. p 862.

Jiang X, Bishop EJ, Farid RS. 1997. A de novo designed protein with properties that characterize natural hyperthermophilic proteins. *J Am Chem Soc 119*:838–839.

Johansson JS, Gibney BR, Skalicky JJ, Wand AJ, Dutton PL. 1998. A native-like three helix bundle protein from structure-based redesign: A novel maquette scaffold. *J Am Chem Soc 120*:3881–3886.

Kalsbeck WA, Robertson DE, Pandey RK, Smith KM, Dutton PL, Bocian DF. 1996. Structural and electronic properties of the heme cofactors in a multiheme synthetic cytochrome. *Biochemistry 35*:3429–3438.

Kamtekar S, Schiffer JM, Xiong H, Babik JM, Hecht MH. 1993. Protein design by binary patterning of polar and nonpolar amino-acids. *Science 262*:1680–1685.

Klemba M, Regan L. 1995. Characterization of metal-binding by a designed protein–single ligand substitutions at a tetrahedral Cys_2His_2 site. *Biochemistry 34*:10094–10100.

Kozlov GV, Ogawa MY. 1997. Electron transfer across a peptide-peptide interface within a designed metalloprotein. *J Am Chem Soc 119*:8377–8378.

Lazar GA, Desjarlais JR, Handel TM. 1997. De novo design of the hydrophobic core of ubiquitin. *Protein Sci 6*:1167–1178.

Lipscomb WN, Sträter N. 1996. Recent advances in zinc enzymology. *Chem Rev 96*:2375–2433.

Lu Y, Valentine JS. 1997. Engineering metal-binding sites in proteins. *Curr Opin Struct Biol 7*:485–500.

Mok YK, De Prat Gay G, Butler PJ, Bycroft M. 1996. Equilibrium dissociation and unfolding of the dimeric human papillomavirus strain-16 E2 DNA-binding domain. *Protein Sci 5*:310–319.

Mulholland SE, Gibney BR, Rabanal F, Dutton PL. 1998. Characterization of the fundamental protein ligand requirements of $[4Fe\text{-}4S]^{2+/+}$ clusters using sixteen amino acid peptide maquettes. *J Am Chem Soc 120*:10296–10302.

Munson M, Balasubramanian S, Fleming KG, Nagi AD, O'Brien R, Sturtevant JM, Regan L. 1996. What makes a protein a protein? Hydrophobic core designs that specify stability and structural properties. *Protein Sci 5*:1584–1593.

Munson M, O'Brien R, Sturtevant JM, Regan L. 1994 Redesigning the hydrophobic core of a four-helix-bundle protein. *Protein Sci 3*:2015–2022.

Mutz MW, McLendon GL, Wishart JF, Gaillard ER, Corin AF. 1996. Conformational dependence of electron transfer across de novo designed metalloproteins. *Proc Natl Acad Sci USA 93*:9521–9526.

Nastri F, Lombardi A, Morelli G, Maglio O, D'Auria G, Pedone C, Pavone V. 1997. Hemoprotein models based on a covalent helix-heme-helix sandwich. 1. Design, synthesis, and characterization. *Chem Eur J 3*:340–348.

Nordlund P, Sjoberg BM, Eklund H. 1990. 3-Dimensional structure of the free-radical protein of ribonucleotide reductase. *Nature 345*:593–598.

Pace CN. 1986. Determination and analysis of urea and guanidine hydrochloride denaturation curves. *Methods Enzymol 131*:266–280.

Peisach J, Blumberg WE, Adler A. 1973. Electron paramagnetic resonance studies of iron porphin and chlorin systems. *Ann NY Acad Sci 206*:310–327.

Pilloud DL, Rabanal F, Gibney BR, Farid RS, Dutton PL, Moser CC. 1998. Self-assembled monolayers of synthetic hemoproteins on silanized quartz. *J Phys Chem B 102*:1926–1937.

Pinto AL, Hellinga HW, Caradonna JC. 1997. Construction of a catalytically active iron superoxide dismutase by rational protein design. *Proc Natl Acad Sci USA 94*:5562–5567.

Price NC, Dwek RA. 1979. *Principles and problems in physical chemistry for biochemists*, 2nd ed. Oxford: Oxford University Press.

Rabanal F, DeGrado WF, Dutton PL. 1996. Toward the synthesis of a photosynthetic reaction center maquette: A cofacial porphyrin pair assembled between two subunits of a synthetic four-helix bundle multiheme protein. *J Am Chem Soc 118*:473–474.

Rau HK, DeJonge N, Haenel W. 1998. Modular synthesis of de novo-designed metalloproteins for light-induced electron transfer. *Proc Natl Acad Sci USA 95*:11526–11531.

Rau HK, Haehnel W. 1998. Design, synthesis, and properties of a novel cytochrome *b* model. *J Am Chem Soc 120*:468–476.

Regan L, Clarke ND. 1990. A tetrahedral Zinc(ii)-binding site introduced into a designed protein. *Biochemistry 29*:10878–10883.

Rivera M, Wells MA, Walker FA. 1994. Cation-promoted cyclic voltammetry of recombinant rat outer mitochondrial-membrane cytochrome b_5 at a gold electrode modified with beta-mercaptopropionic acid. *Biochemistry 33*:2161–2170.

Robertson DE, Farid RS, Moser CC, Urbauer JL, Mulholland SE, Pidikiti R, Lear JD, Wand AJ, DeGrado WF, Dutton PL. 1994. Design and synthesis of multi-heme proteins. *Nature 368*:425–432.

Robinson CR, Liu Y, Thomson JA, Sturtevant JM, Sligar SG. 1997. Energetics of heme binding to native and denatured states of cytochrome b_{562}. *Biochemistry 36*:16141–16146.

Rojas NRL, Kamtekar S, Simons CT, Mclean JE, Vogel KM, Spiro TG, Farid RS, Hecht MH. 1997. De novo heme proteins from designed combinatorial libraries. *Protein Sci 6*:2512–2524.

Rosenzweig AC, Frederick CA, Lippard SJ, Nordlund P. 1993. Crystal-structure of a bacterial nonheme iron hydroxylase that catalyzes the biological oxidation of methane. *Nature 366*:537–543.

Roy S, Ratnaswamy G, Boice JA, Fairman R, McLendon G, Hecht MH. 1997. A protein designed by binary patterning of polar and nonpolar amino acids displays native-like properties. *J Am Chem Soc 119*:5302–5306.

Schafmeister CE, LaPorte SL, Miercke LJW, Stroud RM. 1997. A designed four helix bundle protein with native-like structure. *Nat Struct Biol 4*:1039–1046.

Sharp RE, Rabanal F, Moser CC, Dutton PL. 1998. Design, synthesis, and characterization of a photoactivatable flavocytochrome molecular maquette. *Proc Natl Acad Sci USA 95*:10465–10470.

Shifman JM, Moser CC, Kalsbeck WA, Bocian DF, Dutton PL. 1998. Functionalized de novo designed proteins: Mechanisms of proton coupling to oxidation/reduction in heme protein maquettes. *Biochemistry 37*:16815–16827.

Skalicky JJ, Gibney BR, Rabanal F, Beiber-Urbauer R, Dutton PL, Wand AJ. 1999. Solution structure of a designed four-α-helix bundle maquette scaffold. *J Am Chem Soc 121*:4941–4951.

Stellwagen E. 1978. Haem exposure as the determinate of oxidation-reduction potential of haem proteins. *Nature 275*:73–74.

Taylor CPS. 1977. The EPR of low spin heme complexes. *Biochim Biophys Acta 491*:137–149.

Trumpower BL. 1990. *J Biol Chem 265*:11409–11412.

Walker FA, Huynh BH, Scheidt WB, Osvath SR. 1986. Models for cytochromes *b*. Effect of axial ligand plane orientation on the EPR and Mössbauer spectra of low-spin ferrihemes. *J Am Chem Soc 108*:5288–5297.

Ward KB, Hendrickson WA, Klippenstein GL. 1975. Quaternary and tertiary structure of haemerythrin. *Nature 257*:818–821.

Xia D, Yu CA, Kim H, Xia JZ, Kachurin AM, Zhang L, Yu L, Deisenhofer J. 1997. Crystal structure of the cytochrome bc_1 complex from bovine heart mitochondria. *Science 277*:60–66.

Zhang Z, Huang L, Shulmeister VM, Chi YI, Kim KK, Hung LW, Crofts AR, Berry EA, Kim SH. 1998. Electron transfer by domain movement in cytochrome bc_1. *Nature 392*:677–684.